Licentiate thesis

Modulation of amyloid β peptide self-assembly: Aggregation mechanisms associated with Alzheimer's disease

Axel Abelein

Supervisor: Prof. Astrid Gräslund

Stockholm University

Department of Biochemistry and Biophysics

2013

Abstract

Self-assembly of the amyloid β peptide ($A\beta$) is strongly linked to the pathogenesis of Alzheimer's disease. Modulation of this aggregation process by small molecule compounds has been shown to potentially inhibit or redirect this process. Thus, a detailed understanding of the mechanism of action of such aggregation modulators is crucial for specific design of therapeutics against amyloidosis diseases. The interaction of small molecules, such as lacmoid, Congo red or surfactants, and $A\beta$ have been investigated in this licentiate thesis using a broad range of biophysical techniques. Here, we characterize the formation and exchange kinetics of soluble dynamic co-aggregates that are formed by $A\beta$ and the aggregation modulators. Alongside a slow fibrillation process of $A\beta$ in the time scale of minutes to hours, dynamic exchange between free and co-aggregate bound peptide occurs on a much faster time scale (micro- to milli-seconds). Depending on the different conformational preferences of $A\beta$, aggregation may be promoted or inhibited. β-structure promoting compounds, *e.g.* surfactants at intermediate concentrations, facilitate fibril formation. In contrast, when $A\beta$ adopts a mainly unstructured state in the co-aggregate, as in the presence of lacmoid, transient interactions with free peptide can kinetically redirect $A\beta$ from aggregation. Based on these findings, the molecular mechanism of action of $A\beta$ in the presence of aggregation modulators can be rationalized in terms of exchange and aggregation rates and conformational preferences.

Contents

1 List of publications

I Axel Abelein, Benedetta Bolognesi, Christopher M. Dobson, Astrid Gräslund, Christofer Lendel, "Hydrophobicity and conformational change as mechanistic determinants for non-specific modulators of amyloid β self-assembly", *Biochemistry* **51**, 126-137 (2012)

II Axel Abelein, Lisa Lang, Christofer Lendel, Astrid Gräslund, Jens Danielsson, "Transient small molecule interactions kinetically modulate amyloid β peptide self-assembly", *FEBS Lett* **586**, 3991-95 (2012)

III Axel Abelein, Jørn Døvling Kaspersen, Søren Nielsen, Grethe Vestergaard Jensen, Gunna Christiansen, Jan Skov Pedersen, Jens Danielsson, Daniel Otzen, Astrid Gräslund, "Formation of dynamic soluble surfactant-induced amyloid β co-aggregates", *submitted manuscript*

2 Introduction

2.1 Alzheimer's disease

Alzheimer's disease (AD) is the most common form of neurodegenerative disorder causing irreversible memory dysfunction of the patients [1, 2]. It belongs to the family of protein misfolding diseases that includes devastating disorders such as Huntington's disease and Parkinson's disease [3, 4]. The first description of the disease was provided by the psychiatrist and neuropathologist Alois Alzheimer [5]. Today, AD is the most common form of dementia (more than 50 % of all dementia cases) and worldwide more than 35 million people suffer from this disease [2, 6]. Age is the major risk factor as AD is generally diagnosed in patients over 65 years [2, 6]. One of eight Americans over 65 is diagnosed with the disease and even 45 % of people older than 85 have AD [6]. Most AD cases appear sporadic, which implies that they do not exhibit any family history. In contrast, the familial form of the disease occurs with a prevalence of below 0.1 % and is associated with mutations in the transmembrane amyloid precursor protein (APP) and presenilin 1 and 2 genes [7]. The major genetic determinant for developing sporadic as well as familial late onset AD is the gene dosage of the Apolipoprotein E type 4 allele [8, 9].

2.2 The amyloid β peptide and its relation to AD

One hallmark of AD is deposit of amyloid plaques peptide and neurofibrillar tangles in the brain of AD patients. These plaques consist of aggregates of the amyloid β ($A\beta$) peptide, while aggregated tau protein is the main compound of neurofibrillar tangles [10, 11]. $A\beta$ is produced by enzymatic cleavage of APP which is concentrated in the synapses of neurons and consists of 695-770 amino acids [10]. The cleavage of APP is performed by enzymes called α-, β- and γ-secretases and can be divided into an amyloidogenic and a non-amyloidogenic pathway.

α-secretase cleaves APP extracellularly at a position 83 from the C-terminus and produces a soluble N-terminal fragment αAPP and a C-terminal fragment that remains in the membrane. The C-terminal fragment is cleaved by γ-sectretase to release a fragments termed p3 and intracellular AICD. Importantly, α-secretase cleaves APP in the $A\beta$ region and liberates fragments that do not form fibrils and thus is referred to the non-amyloidogenic pathway [3, 10].

In contrast, the amyloidogenic pathway consists of the β- and γ-secretases. The β-secretases cleave APP at a position 99 from the C-terminus releasing soluble βAPP and the membrane-associated C-terminal fragment. Subsequent γ-secretases liberate 38 to 43 residue long $A\beta$ [3, 10]. The 40 residue long variant, $A\beta_{40}$, is the most prevalent form while the more hydrophobic and aggregation prone 42 residue variant, $A\beta_{42}$, occurs with a proportion of about 10 % [10]. In particular, $A\beta_{42}$ has a high propensity to form oligomeric and fibrillar complexes and it is the predominant species found in amyloid plaques [3, 10]. The $A\beta$ peptide sequence is given by:

$$\mathrm{DAEFR_5HDSGY_{10}EVHHQ_{15}KLVFF_{20}AEDVG_{25}SNKGA_{30}IIGLM_{35}VGGVV_{40}IA_{42}}$$

3 Methods

In this thesis a broad range of biophysical methods has been used including several spectroscopy and microscopy techniques. Spectroscopy generally refers to the measurement of the transitions between different energy levels of electrons or nuclei. Thus, the fundamental basis of all spectroscopic methods is the time-dependent *Schrödinger* equation (TSE):

$$i\hbar\frac{\partial\Psi}{\partial t} = \hat{H}\Psi \tag{1}$$

with the wave function Ψ, the reduced Planck constant $\hbar$ and a characteristic, method-specific Hamiltonian $\hat{H}$ which describes the total energy of the given wave function. In order to handle large spin ensembles the TSE may be rewritten using a density operator[1] $\hat{\rho}$ in form of the *Liouville-von Neumann* (LvN) equation that describes the time evolution of the density operator using the concept of commutators [12, 13]:

$$\frac{d}{dt}\hat{\rho}(t) = \frac{i}{\hbar}[\hat{\rho}(t), \hat{H}(t)] \tag{2}$$

The techniques described in the following sections have been used in this thesis.

3.1 Circular Dichroism (CD)

CD refers to the different absorption of left and right circularly polarized light. Photon absorption may be described by a transition probability $w(0 \rightarrow 1)$ from the ground to an excited state. The transition probability can be calculated writing the Hamiltonian as an time-independent term $\hat{H}^{(0)}$ with a time-dependent perturbation $\hat{H}^{(1)}(t)$ as $\hat{H} = \hat{H}^{(0)} + \lambda\hat{H}^{(1)}(t)$ and is referred to *Fermi's golden rule* [14]. For CD the perturbation term is given by [14]:

$$\hat{H}^{(1)}(t) = -\boldsymbol{\mu}\cdot\mathbf{E}(t) - \mathbf{m}\cdot\mathbf{B}(t) + \textit{higher order terms} \tag{3}$$

in which $\mathbf{E}$ and $\mathbf{B}$ describe the electronic and magnetic field, respectively, with the associated electric $\boldsymbol{\mu}$ and magnetic $\mathbf{m}$ dipole moments.

The difference of absorption coefficients $\Delta\epsilon$ for left and right circularly polarized light is thus given by the difference of transition probabilities [14–16]. Hence, the CD signal, that is proportional to $\Delta\epsilon$, is given in terms of the electric $\boldsymbol{\mu}$ and magnetic $\mathbf{m}$ dipole moments by the Rosenfeld equation [14–17]:

$$\begin{aligned} CD \propto \Delta\epsilon &= \epsilon_L - \epsilon_R && (4)\\ &\propto \Delta w(0\rightarrow 1) = w_L(0\rightarrow 1) - w_R(0\rightarrow 1) && (5)\\ &\propto \Im\left\{\langle\Psi_0|\hat{\boldsymbol{\mu}}|\Psi_1\rangle\cdot\langle\Psi_1|\hat{\mathbf{m}}|\Psi_0\rangle\right\} && (6) \end{aligned}$$

[1] The density operator is defined as $\hat{\rho} = p_j\sum_j|\Psi_j\rangle\langle\Psi_j|$ where p_j gives the probability for the pure state $|\Psi_j\rangle$ and, thus, describes an ensemble average of all spins in the system.

in which Ψ_0 and Ψ_1 are the wave functions of the ground and the first excited state, respectively. The CD signal is hence proportional to the imaginary part of the scalar product of the electric and magnetic dipole moments. For maximal CD signal the electric and magnetic dipole moments are oriented parallel causing a screw-like movement of the electrons. This originates from a combination of translation and rotation that arise from the electric and magnetic dipole moments, respectively [14, 16].

Absorption in the far-UV region (190-260 nm) is caused by energy transitions in the peptide bond, *i.e.* the $\pi \rightarrow \pi^*$ (around 190 nm) and the $n \rightarrow \pi^*$ (around 220 nm) transitions [15, 16, 18]. Secondary structure elements show characteristic CD spectra that can by used to obtain structural information about the protein or peptide [15, 16].

3.2 Fluorescence spectroscopy

Fluorescence is the emission of light caused by electric transition from an excited singlet state (S_1 or S_2) to the ground state S_0 [19]. After light absorption (fluorophore excitation) at an excitation frequency ν_{ex} which is described by $S_0 + h\nu_{ex} \rightarrow S_1$, the electron relaxes from some higher vibrational level to the lowest vibrational level of S_1 or S_2. This process is called internal conversion and causes heat. The transition from the S_1 or S_2 state to an excited vibrational level of the ground state S_0, which relaxes then to the equilibrium state, gives rise to the emission spectrum: $S_1 \rightarrow S_0 + h\nu_{em} + heat$ [19].

Th aromatic amino acids tryptophan, phenylalanine and tyrosine are intrinsic fluorophores where phenylalanine has only about 15 % of the quantum yield of tyrphtophan or tyrosine [19]. $A\beta$ contains three phenylalanines (F4, F19 and F20) and one tyrosine (Y10) that due to the higher quantum yield is used for intrinsic fluorescence experiments.

Besides intrinsic fluorophores fluorogenic probes, such as Thioflavin T (ThT), can be used. ThT may be applied to detect amyloid material as it becomes highly fluorescent when binding to amyloid fibrils [20]. The high fluorescence enhancement of ThT upon binding is caused by a stabilization of the bond between the benzylamine and benzathiole rings. In solution, these rings are allowed to rotated freely which leads to rapid quenching of excited photon states and, thus, drastically decreases fluorescence. In contrast, binding immobilizes the C-C bond between the rings which highly enhances the quantum yield [20, 21]. ThT is commonly applied to monitor kinetics of fibril formation (see section 4.2).

3.3 Nuclear Magnetic Resonance (NMR)

NMR describes the interaction of a nuclear spin with its surrounding environment. The basic principles comprise, first, the alignment of the nucleus spin to an external static magnetic field B_0 and, second, perturbations of this field by applying radio-frequency (rf) pulses. The effect of an electro-magnetic pulse may be described in the form of a Hamiltonian operator $\hat{H} = -\boldsymbol{\mu} \cdot \mathbf{B}(t)$. Hence, the solution of the LvN equation, eq(2), determines the outcome of an NMR experiment and is generally given by:[2]

$$\hat{\rho}(t) = \exp(-i\hat{H}t)\hat{\rho}(0)\exp(i\hat{H}t) \tag{7}$$

Besides rf-pulses the Hamiltonian may contain chemical shift, scalar and dipolar coupling terms. These terms are responsible for chemical shift differences (which makes interpretation of protein NMR possible), multiplet structures of signals and coherence transfers that are essential for multi-dimensional NMR experiments [22].

3.3.1 Relaxation

A basic NMR phenomenon is *relaxation* that describes the return of a non-equilibrium density operator to its original state. This is caused by couplings of nuclear spin with the surrounding environment which creates a local magnetic field $B_{loc}(t)$. The relaxation mechanism is described by the *Redfield* theory where the *Redfied* equation describes the relaxation behavior:

$$\frac{d\hat{\rho}^T(t)}{dt} = -\int_0^\infty \overline{\left[\hat{H}_1^T(t), \left[\hat{H}_1^T(t+\tau), \hat{\rho}^T(t)\right]\right]} d\tau \tag{8}$$

A derivation outline of eq(8) is given in appendix A. Expressions for the longitudinal, R_1, and transverse, R_2, relaxation rates may be derived form eq(8) by introducing the *spectral density function* $J(\omega) = \frac{2}{5}\frac{\tau_c}{(1+\omega^2\tau_c^2)}$ with the resonance frequency ω and correlation time τ_c. $J(\omega)$ is obtained by Fourier transformation of the *time-correlation function* $G(\tau)$, which is defined as the *auto-correlation* of a stochastic fluctuating magnetic field:

$$G(\tau) = \overline{B_{loc}(t)B_{loc}(t+\tau)} \tag{9}$$

$$J(\omega) = \int_{-\infty}^{\infty} G(\tau)\exp(-i\omega\tau)d\tau \tag{10}$$

[2] Eq(7) is a solution to the LvN equation which is shown by:

$$\begin{aligned}\frac{d\hat{\rho}(t)}{dt} &= -\frac{i}{\hbar}\hat{H}\exp(-i\hat{H}t)\hat{\rho}(0)\exp(i\hat{H}t) + \exp(-i\hat{H}t)\hat{\rho}(0)\frac{i}{\hbar}\hat{H}\exp(i\hat{H}t) \\ &\quad \text{with } [\hat{A}, \exp(\hat{A})] = 0 \text{ , } i.e. \ \hat{A} \text{ and } \exp(\hat{A}) \text{ commute} \\ &= -\frac{i}{\hbar}[\hat{H}, \hat{\rho}(t)] = \frac{i}{\hbar}[\hat{\rho}(t), \hat{H}]\end{aligned}$$

The relaxation rates for backbone NH-nuclei are given by [13, 22, 23]:

$$R_1 = \frac{d^2}{4}\left(J(\omega_H - \omega_N) + 3J(\omega_N) + 6J(\omega_H + \omega_N)\right) + c^2 J(\omega_N) \tag{11}$$

$$R_2 = \frac{d^2}{8}\left(4J(0) + J(\omega_H - \omega_N) + 3J(\omega_N) + 6J(\omega_H) + 6J(\omega_H + \omega_N)\right) + \frac{c^2}{6}\left(4J(0) + 3J(\omega_N)\right) \tag{12}$$

with the constants $d = \frac{\mu_0 \gamma_N \gamma_H \hbar}{4\pi r_{NH}^{-3}}$ and $c = \Delta\sigma\,\omega_N/\sqrt{3}$ in which μ_0 is the permeability constant, $\hbar$ the reduced Planck constant, r_{NH} the NH bond length and γ_H and γ_N the gyromagnetic ratios, ω_H and ω_N the larmor frequencies of ^{1}H and ^{15}N, respectively.

3.3.2 Chemical exchange and relaxation dispersion

A general two-site chemical exchange process between the states A and B may be depicted as:

$$A \underset{k_{-1}}{\overset{k_1}{\rightleftharpoons}} B$$

where k_1 and k_{-1} are the first-order rate constants for the forward and reverse transition, respectively. The exchange rate is defined as [24]:

$$k_{ex} = k_1 + k_{-1} = k_1/p_B = k_{-1}/p_A \tag{13}$$

where p_A and p_B are the population for state A and B, respectively. The resonance frequency difference between the two states is given by $\Delta\omega = |\Omega_A - \Omega_B|$ where Ω_A and Ω_B are the resonance frequencies for state A and B, respectively.

The effect of chemical or conformational exchange is described by the Bloch-McConnell equations [25]:

$$\frac{d}{dt}\begin{pmatrix}\tilde{M}_A(t)\\ \tilde{M}_B(t)\end{pmatrix} = \begin{pmatrix}-i\Omega_A - R_{2A}^0 - p_B k_{ex} & p_A k_{ex}\\ p_B k_{ex} & -i\Omega_B - R_{2B}^0 - p_A k_{ex}\end{pmatrix}\begin{pmatrix}\tilde{M}_A(t)\\ \tilde{M}_B(t)\end{pmatrix} \tag{14}$$

in which R_{2A}^0 and R_{2B}^0 are the transverse relaxation rates and $\tilde{M}_A$ and $\tilde{M}_B$ the magnetization in the rotating frame for state A and B, respectively. This differential equation can be solved yielding a coefficient matrix that describes the time-dependence of the start magnetization [24]. Fourier transformation of this solution results in the desired NMR spectrum.

A Carr-Purcell-Meiboom-Gill (CPMG) pulse scheme [26, 27] can be used to record effect of chemical exchange on the transverse relaxation rates. The CPMG pulse sequence consists of a block of 180° pulses with a delay τ_{CP} between two 180° pulses in the $\tau_{CP}/2 - 180° - \tau_{CP}/2$ spin-echo period. The pulse program applied in this study [28] includes a pulse element for exchange of in- and anti-phase magnetization in the middle of the constant time relaxation that is embedded by two CPMG blocks (applied with a

$-\pi/2$ phase shift) with mixing time (or relaxation delay) $T_{CP}/2$ [28,29]. The relaxation rates R_2^{obs} are calculated from the cross-peak amplitudes by:

$$R_2^{obs} = \frac{1}{T_{CP}} \ln\left(\frac{I}{I_0}\right) \tag{15}$$

in which I is the peak heights for different CPMG frequencies, ν_{CPMG}, and I_0 the peak height from the reference experiment recorded at $T_{CP} = 0$ ms.
The transverse relaxation rate R_2 is a function of the interpulse delay $\tau_{CP} = 1/(2\,\nu_{CPMG})$ and is given by [24,30,31]:

$$R_2^{obs}(1/\tau_{CP}) = \frac{1}{2}\left(R_{2A}^0 + R_{2B}^0 + k_{ex} - \frac{1}{\tau_{cp}} \cdot \cosh^{-1}\left[D_+ \cosh(\eta_+) - D_- \cos(\eta_-)\right]\right) \tag{16a}$$

with

$$D_\pm = \frac{1}{2}\left(\pm 1 + \frac{\psi + 2\Delta\omega^2}{(\psi^2 + \xi^2)^{1/2}}\right) \tag{16b}$$

$$\eta_\pm = \frac{\tau_{cp}}{\sqrt{2}}\left(\pm\psi + (\psi^2 + \xi^2)^{1/2}\right)^{1/2} \tag{16c}$$

$$\psi = (R_{2A}^0 - R_{2B}^0 - p_a k_{ex} + p_b k_{ex})^2 - \Delta\omega^2 + 4\,p_A\,p_B\,k_{ex}^2 \tag{16d}$$

and

$$\xi = 2\Delta\omega(R_{2A}^0 - R_{2B}^0 - p_a\,k_{ex} + p_b\,k_{ex}) \tag{16e}$$

where R_{2A}^0 and R_{2B}^0 are the intrinsic transverse relaxation rates of each state without contribution of chemical exchange.

Assuming a model with equal transverse relaxation rates for the two states, which decrease the number of fitting parameters, eq(16) may be simplified by using $R_2^{calc} = R_{2A}^0 = R_{2B}^0$ [29,32] which was applied in paper II and III.

Notably, only the magnitude of the chemical shift is obtained by relaxation dispersion since these experiments are based on exchanged-induced line broadening [33] that does not provide any sign information. However, experiments based on exchange-induced chemical shifts may be used to obtain the sign of the chemical shifts [33], *e.g.* using HSQC/HMQC (Heteronuclear Single/Multiple Quantum Coherence), field-dependent HSQC or $R_{1\rho}$ experiments [33,34]. HSQC/HMQC methods have been shown to be most effective for ^{15}N chemical shifts [34]. However, to obtain significant chemical shift changes the exchange rate should be in the range 100 to 10000 s^{-1} and the minor population $p_B \gtrsim 3$ % [33]. Recent studies showed that even slower exchange regimes can be investigated using chemical exchange saturation transfer methods [35,36].

Taken together, CPMG relaxation dispersion experiments can provide information about intrinsic relaxation rates, which may be used for size estimates of the complex for the bound state (paper II and III), dynamics of the system (via the exchange rate k_{ex}), structural properties of the states (via the chemical shift difference $|\Delta\omega|$ in ppm units) and thermodynamics (via the populations p_A and p_B with exchange rate k_{ex}).

4 Aggregation pathways

4.1 Aggregation process

Amyloid formation, which refers to formation of insoluble protein aggregates, can be described as a polymerization reaction that is governed by a set of microscopic rate constants [37,38]. Hydrophobicity, secondary structure propensity for β-sheet formation and charge determine the aggregation rates of amyloidogenic peptides and proteins [39,40]. In particular, the hydrophobic stretches in $A\beta$ peptide sequence promote aggregation [41].

Mature fibrils are the final aggregation state and feature a so called cross-β structure, where the β strands run perpendicular to the fibril axis, as revealed by solid-state NMR [42–44]. Hence, a conformational conversion from an initial random coil-like state [45] into a β-sheet structure occurs during the aggregation process. Early assemblies of oligomeric $A\beta$ are in particular focus as they have been suggested to cause neuronal damage [3,7]. These early stage oligomers may either be rather loosely structured or feature a high β-structure content [46–48]. Besides oligomers that occur on-pathway to fibril formation, other oligomeric species may appear off-pathway [49,50]. There is evidence that the aggregation pathway, and thus the formation of certain kinds of oligomers, can be influenced and regulated by aggregation modulators (section 4.3). Figure 1 shows a simplified schematic model for $A\beta$ aggregation pathways. Here, monomeric peptides assemble to relatively small oligomeric aggregates that may either be on- or off-pathway to fibril formation. The aggregates (oligomers) that occur on-pathway convert to β-rich oligomeric aggregates that are prone to form fibrils [4,51]. The intrinsic β-turn propensity of the residues 24 to 28 may lead to a nucleation of β-sheet formation [48,52]. The β-rich aggregates that occur as the pre-fibrillar species may be so called protofibrils that show curvilinear structures structure in transmission electron microscopy (TEM) and interact with amyloid-binding dyes [51]. Yet, also other pre-fibrillar intermediates with a spherical form have been reported to form fibrils [7,48,53].

A large number of intermediate $A\beta$ assemblies that show different degrees of synaptoxicity have been reported in literature (reviewed in [3,7]). In addition, it is not clear how oligomers studied *in vitro* are linked to the appearance of oligomers *in vivo* as *in vitro*-oligomers are often generated under simplified, non-physiological conditions [3,7].

4.2 Aggregation kinetics

Protein/peptide self-assembly is governed by primary nucleation reactions, which describe aggregate formation from soluble monomers, and/or secondary nucleation pathways, such as fragmentation and surface catalyzed nucleation [37,38]. The kinetics of fibril formation can be monitored by optical spectroscopy, *e.g.* fluorescence spectroscopy using amyloid-binding dyes such as ThT [20]. The kinetic profiles generally show an exponential or sigmoidal shape[3] for non-seeded aggregation where the slope of the time course reaction is proportional to the concentration of monomers [38]. Beside

[3]Sigmoidal kinetic traces are described by $S(t) = B + A/\left(1+\exp(-k(t-t_{1/2}))\right)$ where A and B describe the amplitude and the base line level, respectively.

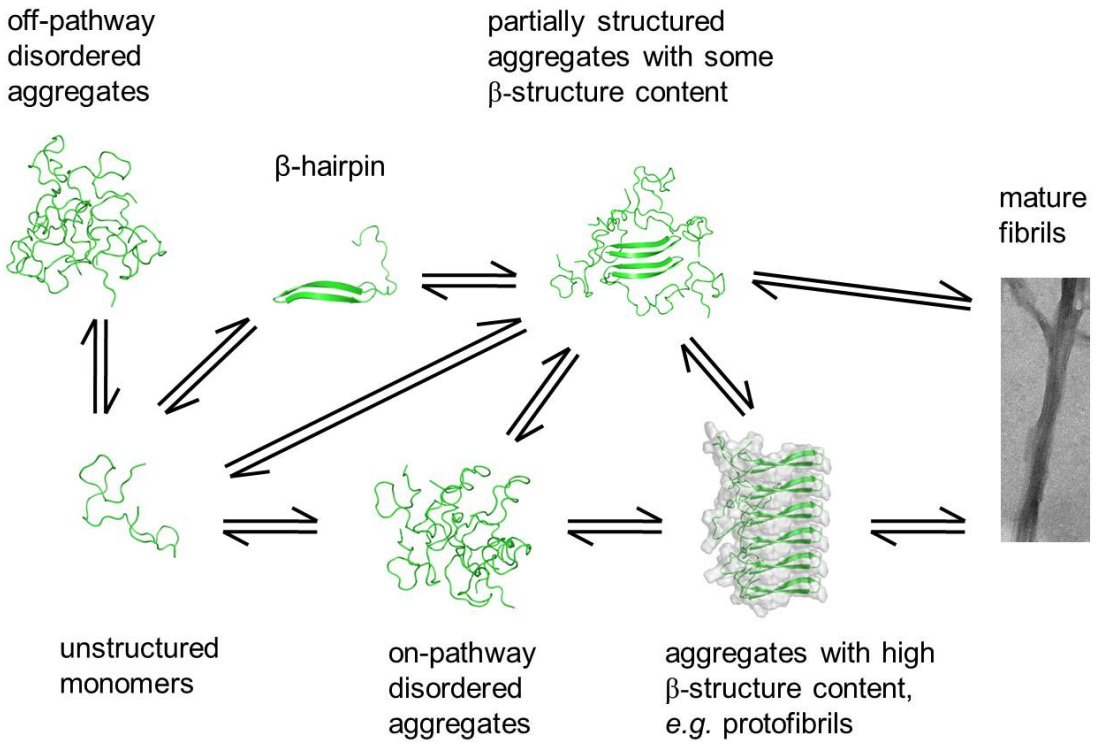

Figure 1: Schematic model for $A\beta$ aggregation pathways [4, 7, 48]. The mature fibril may be formed from aggregated states and monomers.

the reaction rate, k, the half time $t_{1/2}$ (time of half completion of aggregation) and the lag time[4] t_{lag} characterize the kinetics. The $t_{1/2}$ is related to the initial monomer concentration c by $t_{1/2} \propto c^{\gamma}$ [38, 54] where the power γ describes in a simplified picture the size of the nucleus (number of peptides in the aggregation nucleus) [55] but more generally reveals the reaction order of the dominant process that leads to creation of new aggregates [38, 56, 57]. For $A\beta_{42}$ the power coefficient γ is in the order of -1.5 to -1.2 [54, 58]. Kinetics of primary (*i.e.* primary nucleation, elongation and dissociation) and secondary pathways (*i.e.* fragmentation and monomer-dependent secondary nucleation) can generally be described by a set of coupled non-linear differential equations where rate constants and nucleus sizes[5] characterize the different processes [37, 56].

Alongside ThT other fluorescent dyes can be used that may detect other earlier aggregation states, such as 1-anilinonaphthalene 8-sulfonate (ANS) that detects rather non-specific or exposed hydrophobic regions [59]. Using fluorophore-labeled $A\beta$ early oligomerization can be monitored that does not give rise to ThT fluorescence [60]. Besides fluorescence methods other techniques, such as CD and dynamic light scattering [61], can be applied to record the time course of $A\beta$ aggregation.

[4]The lag time is related to the rate constant k and the $t_{1/2}$ time by $t_{lag} = t_{1/2} - 2/k$ [54].

[5]Nucleus sizes for primary nucleation (n_c) and monomer-dependent secondary nucleation (n_2) [37,56]

4.3 Aggregation modulators

A large number of compounds have been shown to modulate protein/peptide aggregation and, hence, might potentially be applicable as therapeutics against amyloidosis diseases and for a detailed understanding of the underlying aggregation mechanism [62,63]. Different mechanisms for aggregation inhibition are reported depending on the strength and specificity of the peptide and/or peptide aggregate-inhibitor interaction [63]. Inhibitors may interact with monomeric peptide, oligomeric or fibrillar species and thereby prevent further peptide self-assembly. Binding to monomeric $A\beta$ was shown for an Affibody protein [64] which inhibits fibrillization by stabilizing a β-hairpin in the monomeric peptide [65].

Besides blocking the $A\beta$ self-assembly, aggregation modulators can promote alternative aggregation pathways. Peptide self-assembly can be redirected from fibrillogenic (on-pathway) oligomers to formation of non-fibrillogenic oligomers, *i.e.* oligomers that appear off-pathway to fibril formation. One such modulator is polyphenol (-)-epigallochatechin gallate (ECGC) - a substance contained in green tea - that promotes formation of oligomers, that lack a pronounced secondary structure, and prevents β-struture formation in $A\beta$ and αSN [66].

Alternatively, conversion from toxic forms of oligomers to amyloid fibrils, which might be non- or less toxic than intermediate pre-fibrillar species, can be accelerated by aggregation modulators. This process was revealed for a related small molecule O4 [67]. Also Congo red (CR), a compound commonly used for amyloid-staining, belongs to this kind of amyloid modulators. CR promotes a β-structure conformation and thereby accelerates fibril formation [68]. In fact, CR may reduce cell toxicity of $A\beta$ by this mechanism [69–71].

Various other examples of small molecule modulators have been reported to inhibit $A\beta$ aggregation [49,72]. Necula *et al.* showed that $A\beta$ inhibitors can specifically prevent oligomer or/and fibril formation which, thus, suggests that these inhibitors interact with distinct oligomeric species that occur on- or off-pathway to fibril formation [49]. Lacmoid, a compound that inhibits both oligomerization and fibrillization [49], forms colloidal aggregates by its own ([73] and paper I) which is a common property among many small-molecule inhibitors [74]. The propensity to form colloidal structures, which is also referred to as a surfactant-like property, may be assigned to the hydrophobic or amphipathic character of the compounds that is a common feature among many small-molecule inhibitors ([74] and paper I).

Different approaches for inhibitor selection have been presented using either high-throughput screening of existing drug libraries [75] or specific chemical and structural design of amyloid inhibitors [76] where the latter requires a more detailed understanding of the mechanism of action.

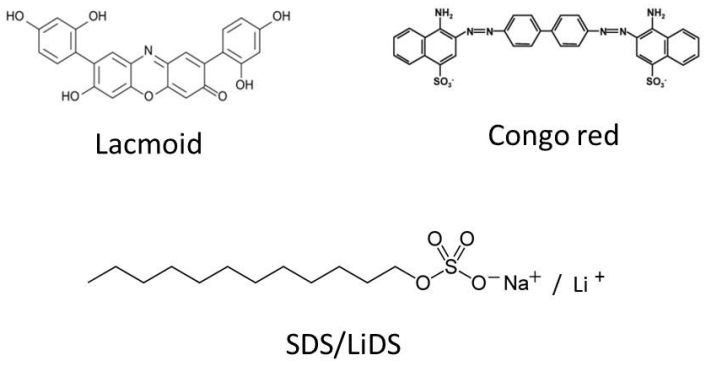

Figure 2: Chemical structures of the small molecule aggregation modulators lacmoid and CR and the surfactants SDS/LiDS

5 Results and Discussion

A detailed understanding of the mechanism of action of different aggregation modulators has been the aim of the papers included in this licentiate thesis. Two small molecule modulators, lacmoid and CR, have been studied in detail as representatives of the class of small molecule inhibitors (paper I and II). As these inhibitors often exhibit colloidal/surfactant-like properties ([74] and paper I) the aggregation process of $A\beta$ in the presence of anionic surfactants, such as sodium/lithium dodecyl sulfate (SDS/LiDS), has been investigated (paper III).

We found that lacmoid binds to $A\beta$ in a non-specific manner causing an overall attenuation of ^{1}H-^{15}N-HSQC and ^{1}H-^{15}N transverse relaxation optimized spectroscopy (TROSY) signals along the whole peptide sequence. Lacmoid inhibits $A\beta$ aggregation demonstrated by kinetic ThT fluorescence, CD and ^{1}H-^{15}N-HSQC experiments in agreement with other studies [49, 72]. $A\beta$ in the presence of high lacmoid concentration (500 μM) remains its random coil characteristics monitored by CD even after peroid of 26 days, while $A\beta$ alone shows a conformational change to a β-structure in the same period. $A\beta$ alone shows significantly more NMR signal loss of monomeric $A\beta$ than the presence of lacmoid. Also TEM images on $A\beta$ samples with and without lacmoid give additional evidence for the inhibitory effect of lacmoid which prevents fibril formation and leads to an overall reduced amount of aggregated material. The exchange rates between $A\beta$ amide hydrogen atoms and water are different along the amino peptide sequence ($k_{NH-H_2O} \sim 2$ to 10 s^{-1}) but do not change by addition of lacmoid. However, conclusions about structural changes are not possible if the chemical exchange rate k_{ex} is much larger than the intrinsic exchange rate $k^{int}_{NH-H_2O}$ as found in paper II. The binding of $A\beta$ to lacmoid is weak compared to the interaction strength when binding to *e.g.* SDS micelles.

$A\beta$ and lacmoid form small-sized co-aggregates that are in dynamic exchange with free peptide. ^{15}N CPMG relaxation dispersion experiments reveal that NMR signal attenuation can be attributed to chemical exchange on an NMR intermediate time scale

[24] with an exchange rate k_{ex} of 1000 s^{-1}. Only a small fraction of $A\beta$ is bound in the co-aggregates. The chemical shift differences show low and uniform magnitudes involving the two hydrophobic parts in the peptide sequence as well as the hydrophilic N-terminus. This indicates that the peptide remains rather unstructured in complex with lacmoid which is in agreement with CD results. The overall formation of co-aggregates is on a slow time scale with an aggregation rate of $k_{co,agg} \sim 11\,s^{-1}$ as monitored by intrinsic tyrosine (Y10) fluorescence experiments. Assuming a spherical co-aggregate with a 1:2 $A\beta$:lacmoid ratio the hydrodynamic radius may be estimated to 43 Å which corresponds to about 50 peptides bound in the co-aggregate.

$A\beta$ in the presence of CR forms also dynamic co-aggregates showing similar exchange kinetics ($k_{ex} \sim 1050\,s^{-1}$) as in the lacmoid case. Yet, CR promotes a β-structure in the peptide as shown by CD experiments [68] and, thus, indicates that the structural states of $A\beta$ in the co-aggregates are different. Also CR forms smaller co-aggregates (r $\sim$ 28 Å) with $A\beta$ than lacmoid.

These findings suggest that dynamic exchange with co-aggregates kinetically redirects monomeric $A\beta$ from self-assembly. Hence, the fast exchange kinetics may explain the inhibitory effect of lacmoid on $A\beta$ aggregation. The conformational preferences of CR to form β-structure promotes fibril formation and, thus, counteracts the effect of the exchange dynamics.

Surfactants induce a secondary structure change in $A\beta$ depending on the surfactant concentration as reported previously [77]. While at low surfactant concentration $A\beta$ is predominately unstructured, $A\beta$ adopts at an intermediate surfactant concentration (c $\sim$ 1-3 mM) a β-structure conformation [77]. Above the critical micelle concentration of the surfactant $A\beta$ forms an α-helical structure. In paper III we investigate the β-structure state as amyloidogenic intermediates along the aggregation pathway were shown to adopt this structure [4].

The fluorophore pyrene can be used to monitor hydrophobic environment [78, 79] which is shown here to be created upon β-structure induction in the peptide. The ratio of two specific emission peaks is dependent on surfactant concentration and shows emission plateaus that correlate with β-structure formation detected by CD. Thus, surface exposed hydrophobic clusters are created when a β-structure is induced in the peptide.

Kinetic measurements using the amyloid-detecting dye ThT demonstrate that β-structure induced at intermediate surfactant concentration is the most aggregation prone state, while the α-helical state induced at high surfactant concentration completely inhibits peptide aggregation.

Small-angle X-ray experiments reveal an initial mixture of small spherical structures and elongated cylinders (length $>$ 350 Å) in a sample with a β-structure inducing surfactant concentration. The cylindrical fibrils grow in radius on a time scale of hours to a final diameter of $\sim$ 60 Å while the spherical aggregates gradually vanish and fibrils are formed during the slow aggregation process. $A\beta$ in the presence of 10 mM SDS (above the cmc) spherical core-shell structures are found indicating that the peptide is bound to the micelle surface as previously reported by NMR studies [80].

The SAXS results are also in agreement with TEM images that display elongated fibrils with a diameter of 50-70 Å at a β-structure inducing SDS concentration. At

high SDS concentrations the amount of aggregated material is substantially reduced, however, some single fibrils are present as well.

The formed $A\beta$-surfactant co-aggregates are dynamic and $A\beta$ show exchange rates ($k_{ex} \sim 1100\ s^{-1}$) between free and bound states on the same time scale as found for $A\beta$ in co-aggregates with lacmoid or CR. Effects on chemical shifts are mainly present in the two hydrophobic parts that are involved in β-structure formation [42,65]. A size estimate from NMR relaxation parameters reveals similar size dimensions as the spherical fraction determined by the SAXS experiments. This suggests that both methods report on the same species and, hence, a small fraction (~ 1 %) of monomeric $A\beta$ undergoes dynamic exchange with spherical co-aggregated oligomers.

These findings can be rationalized in a model where free peptide transiently binds to dynamic spherical co-aggregates. These co-aggregates slowly disappear during the aggregation process and elongated fibrils are formed on a minute to hour time scale.

6 Conclusions

The mechanism of action of $A\beta$ self-assembly and the influence of aggregation modulators on this process have been investigated in this thesis. Hydrophobic attraction and conformational preferences of $A\beta$ in the presence of small molecule aggregation modulators were identified to be major determinants of their mechanism of interaction. The property of many aggregation modulators to form colloidal aggregates by its own ("surfactant-like") motivates a strong link to $A\beta$-surfactant interactions. Both small molecules and surfactants form dynamic soluble co-aggregates with $A\beta$ which may be depicted as simplified micelles. A small fraction of $A\beta$ bound to the co-aggregate undergoes rapid dynamic exchange with free peptide. These transient interactions kinetically modulate the $A\beta$ self-assembly. When $A\beta$ adopts a predominant disorder state in the co-aggregates, as in the presence of lacmoid, formation of dynamic co-aggregates may inhibit $A\beta$ aggregation. In contrast, aggregation modulators that favor a β-structure in $A\beta$, such as surfactants at intermediate concentrations, generally promote aggregation and fibril formation. While fibril formation occurs on a slow time scale (minutes to hours), dynamic exchange between free and co-aggregated bound peptide is on a much faster time scale (micro- to milli-seconds).

Taken together, the molecular mechanism of action of $A\beta$ in the presence of aggregation modulators that exhibit colloidal properties may be rationalized in terms of exchange and aggregation rates and conformational preference of $A\beta$ (Figure 3). These findings might potentially be helpful for design of therapeutics against amyloidosis diseases.

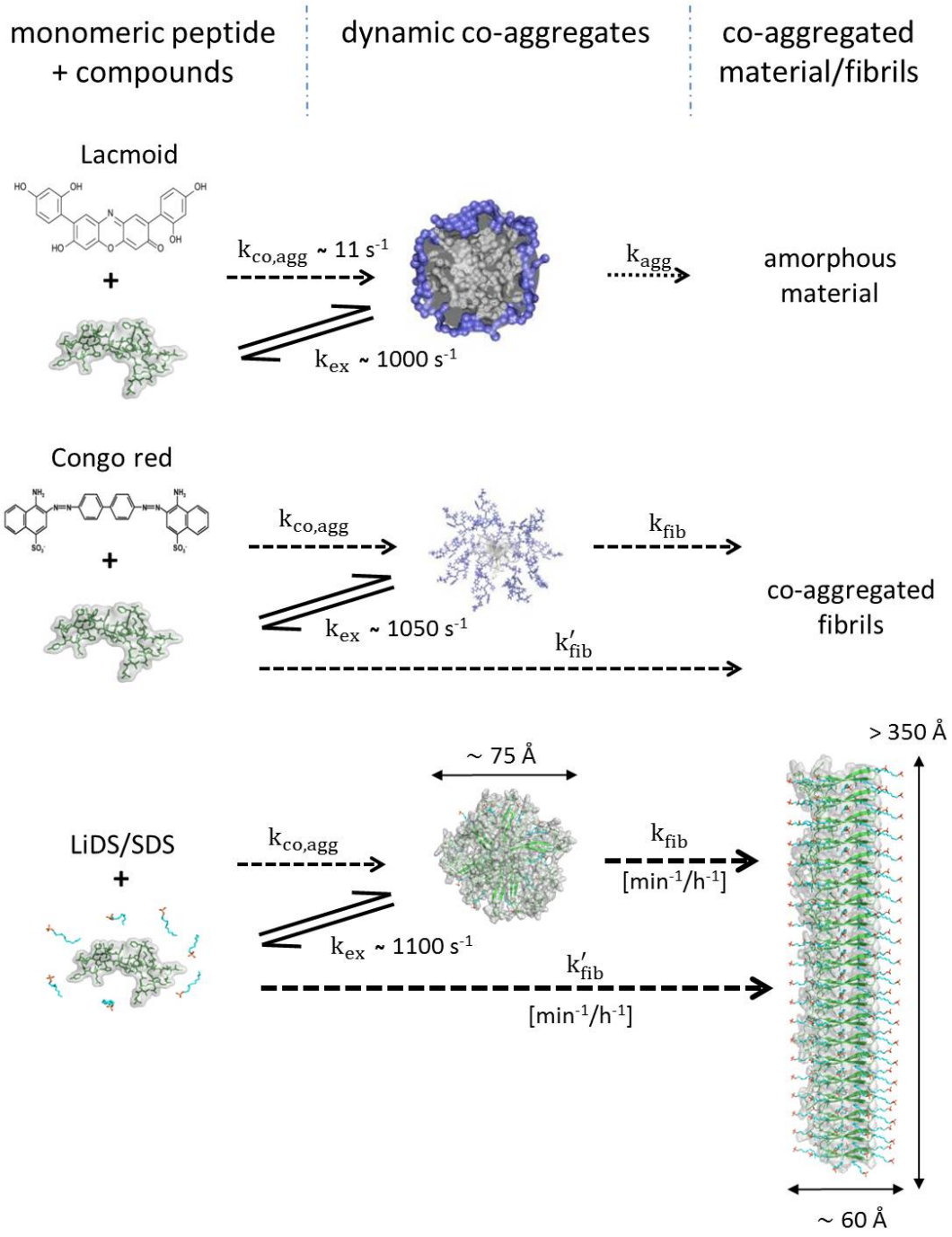

Figure 3: Schematic effects by lacmoid, CR and SDS/LiDS on $A\beta$ self-assembly. $A\beta$ and these compounds form soluble dynamic co-aggregates with a formation rate $k_{co,agg}$, which are depicted as spherical micelles. Free and co-aggregate bound peptides undergo rapid exchange with an exchange rate in the order of 1000 s^{-1}. $A\beta$ in the presence of lacmoid is mainly unstructured in the co-aggregate and transient interactions with free peptide kinetically redirect $A\beta$ from self-assembly. In contrast, $A\beta$ in the presence of CR and LiDS/SDS adopts a β-structure rich state which facilitates fibril formation. The slow fibrillation process occurs on a time scale of minutes to hours.

Acknowledgments

During my time at the Department of Biochemistry and Biophysics I had the pleasure to cooperate with and get support from many people. In particular, I would like to acknowledge:
Astrid Gräslund, for supervising me through the past years with fruitful inspiration and encouraging support.
Jens Danielsson, for your introduction to NMR relaxation dispersion and aggregation kinetics, and co-supervision of my recent projects.
Christofer Lendel, for introducing me to small molecule aggregation modulators and co-supervising my first project.
All co-workers in the past projects, for your work and effort to finalize the projects and the methods I learned from you.
Jüri Jarvet and Sebastian Wärmländer, for your continuous help, support and discussions concerning $A\beta$.
Torbjörn and Haidi Astlind, for great technical and administrative support!
Lena Mäler and Andreas Barth, for valuable advice and discussion about NMR and infra red.
My present and past PhD colleagues in the NMR biophysics group: Jobst, Johannes, Weihua, Sofia, Fatemeh, Scarlett and Anna, for discussing and helping with daily problems in the lab and analysis but in particular for creating such a wonderful atmosphere in the biophysics corridor. It is a pleasure and great fun to be here and have you around!!!
Everyone at DBB, for such a nice scientific environment and working atmosphere.

References

[1] Citron, M. Alzheimer's disease: strategies for disease modification. *Nat Rev Drug Discov* **9**, 387–398 (2010). URL http://dx.doi.org/10.1038/nrd2896.

[2] Querfurth, H. W. & LaFerla, F. M. Alzheimer's disease. *N Engl J Med* **362**, 329–344 (2010). URL http://dx.doi.org/10.1056/NEJMra0909142.

[3] Haass, C. & Selkoe, D. J. Soluble protein oligomers in neurodegeneration: lessons from the Alzheimer's amyloid beta-peptide. *Nat Rev Mol Cell Biol* **8**, 101–112 (2007). URL http://dx.doi.org/10.1038/nrm2101.

[4] Chiti, F. & Dobson, C. M. Protein misfolding, functional amyloid, and human disease. *Annu Rev Biochem* **75**, 333–366 (2006). URL http://dx.doi.org/10.1146/annurev.biochem.75.101304.123901.

[5] Alzheimer, A. Über eine eigenartige Erkrankung der Hirnrinde. *Allg. Z. Psychiat. Psych.-Gerichtl. Med* **64**, 146–148 (1907).

[6] Alzheimer's association. Annual report 2012: Alzheimer's disease facts and figures (2012). URL http://www.alz.org/downloads/facts_figures_2012.pdf.

[7] Benilova, I. & De Strooper, B. An overlooked neurotoxic species in alzheimer's disease. *Nat Neurosci* **14**, 949–950 (2011). URL http://dx.doi.org/10.1038/nn.2871.

[8] Corder, E. H. *et al.* Protective effect of apolipoprotein e type 2 allele for late onset Alzheimer disease. *Nat Genet* **7**, 180–184 (1994). URL http://dx.doi.org/10.1038/ng0694-180.

[9] Reiman, E. M. *et al.* Fibrillar amyloid-beta burden in cognitively normal people at 3 levels of genetic risk for Alzheimer's disease. *Proc Natl Acad Sci U S A* **106**, 6820–6825 (2009). URL http://dx.doi.org/10.1073/pnas.0900345106.

[10] LaFerla, F. M., Green, K. N. & Oddo, S. Intracellular amyloid-beta in Alzheimer's disease. *Nat Rev Neurosci* **8**, 499–509 (2007). URL http://dx.doi.org/10.1038/nrn2168.

[11] Aguzzi, A. & O'Connor, T. Protein aggregation diseases: pathogenicity and therapeutic perspectives. *Nat Rev Drug Discov* **9**, 237–248 (2010). URL http://dx.doi.org/10.1038/nrd3050.

[12] Sakurai, J. *Modern Quantum Mechanics* (Addison-Wesley Publishing Company, 1994).

[13] Kowalewski, J. & Mäler, L. *Nuclear spin relaxation in liquids: theory, experiments, and applications*, vol. 2 (Taylor & Francis, 2006).

[14] Berova, N., Nakanishi, K. & Woody, R. W. *Circular Dichroism - Principles and Applications* (WILEY-VCH, 2000).

[15] Rodger, A. & Nordén, B. *Circular Dichroism and Linear Dichroism* (Oxford University Press, 1997).

[16] Fasman, G. D. *Circular Dichroism and the Conformational Analysis of Biomolecules* (Plenum Publishing Corporation, 1996).

[17] Rosenfeld, L. Quantenmechanische Theorie der natürlichen optischen Aktivität von Flüssigkeiten und Gasen. *Zeitschrift für Physik* **52**, 161–174 (1929). URL http://dx.doi.org/10.1007/BF01342393.

[18] Abelein, A. *Biophysical studies of the amyloid β peptide: Aggregation mechanisms associated with Alzheimer's disease*. Master thesis, Stockholm University (2010).

[19] Lakowicz, J. R. *Principles of Fluorescence Spectroscopy* (Springer, 2006).

[20] Biancalana, M. & Koide, S. Molecular mechanism of Thioflavin-T binding to amyloid fibrils. *Biochim Biophys Acta* **1804**, 1405–1412 (2010). URL http://dx.doi.org/10.1016/j.bbapap.2010.04.001.

[21] Stsiapura, V. I., Maskevich, A. A., Kuzmitsky, V. A., Turoverov, K. K. & Kuznetsova, I. M. Computational study of thioflavin T torsional relaxation in the excited state. *J Phys Chem A* **111**, 4829–4835 (2007). URL http://dx.doi.org/10.1021/jp070590o.

[22] Cavanagh, J., Fairbrother, W. J., Palmer, A. G. & Skelton, N. J. *Protein NMR Spectroscopy: Principles and Practice* (Academic Press, 1996).

[23] Palmer, A., 3rd. NMR probes of molecular dynamics: overview and comparison with other techniques. *Annu Rev Biophys Biomol Struct* **30**, 129–155 (2001). URL http://dx.doi.org/10.1146/annurev.biophys.30.1.129.

[24] Palmer, A., 3rd, Kroenke, C. D. & Loria, J. P. Nuclear magnetic resonance methods for quantifying microsecond-to-millisecond motions in biological macromolecules. *Methods Enzymol* **339**, 204–238 (2001).

[25] McConnell, H. M. Reaction rates by nuclear magnetic resonance. *J Chem Phys* **28**, 430–431 (1958). URL http://link.aip.org/link/?JCP/28/430/1.

[26] Carr, H. Y. & Purcell, E. M. Effects of diffusion on free precession in nuclear magnetic resonance experiments. *Phys Rev* **94**, 630–638 (1954).

[27] Meiboom, S. & Gill, D. Modified spin-echo method for measuring nuclear relaxation times. *Review of Scientific Instruments* **29**, 688–691 (1958).

[28] Tollinger, M., Skrynnikov, N. R., Mulder, F. A., Forman-Kay, J. D. & Kay, L. E. Slow dynamics in folded and unfolded states of an SH3 domain. *J Am Chem Soc* **123**, 11341–11352 (2001). URL http://pubs.acs.org/doi/abs/10.1021/ja011300z.

[29] Korzhnev, D. M., Karlsson, B. G., Orekhov, V. Y. & Billeter, M. NMR detection of multiple transitions to low-populated states in azurin. *Protein Sci* **12**, 56–65 (2003). URL http://dx.doi.org/10.1110/ps.0225403.

[30] Carver, J. & Richards, R. A general two-site solution for the chemical exchange produced dependence of T_2 upon the Carr-Purcell pulse separation. *J Magn Reson* **6**, 89–105 (1972).

[31] Davis, D. G., Perlman, M. E. & London, R. E. Direct measurements of the dissociation-rate constant for inhibitor-enzyme complexes via the $T_{1\rho}$ and T_2 (CPMG) methods. *J Magn Reson B* **104**, 266–275 (1994). URL http://dx.doi.org/10.1006/jmrb.1994.1084.

[32] Kovrigin, E. L., Kempf, J. G., Grey, M. J. & Loria, J. P. Faithful estimation of dynamics parameters from CPMG relaxation dispersion measurements. *J Magn Reson* **180**, 93–104 (2006). URL http://dx.doi.org/10.1016/j.jmr.2006.01.010.

[33] Skrynnikov, N. R., Dahlquist, F. W. & Kay, L. E. Reconstructing NMR spectra of invisible excited protein states using HSQC and HMQC experiments. *J Am Chem Soc* **124**, 12352–12360 (2002). URL http://pubs.acs.org/doi/abs/10.1021/ja0207089.

[34] Auer, R. *et al.* Measurement of signs of chemical shift differences between ground and excited protein states: a comparison between H(S/M)QC and $R_{1\rho}$ methods. *J Biomol NMR* **46**, 205–216 (2010). URL http://dx.doi.org/10.1007/s10858-009-9394-z.

[35] Fawzi, N. L., Ying, J., Ghirlando, R., Torchia, D. A. & Clore, G. M. Atomic-resolution dynamics on the surface of amyloid-β protofibrils probed by solution NMR. *Nature* **480**, 268–272 (2011). URL http://dx.doi.org/10.1038/nature10577.

[36] Vallurupalli, P., Bouvignies, G. & Kay, L. E. Studying "invisible" excited protein states in slow exchange with a major state conformation. *J Am Chem Soc* **134**, 8148–8161 (2012). URL http://dx.doi.org/10.1021/ja3001419.

[37] Knowles, T. P. J. *et al.* An analytical solution to the kinetics of breakable filament assembly. *Science* **326**, 1533–1537 (2009). URL http://dx.doi.org/10.1126/science.1178250.

[38] Cohen, S. I. A., Vendruscolo, M., Dobson, C. M. & Knowles, T. P. J. From macroscopic measurements to microscopic mechanisms of protein aggregation. *J Mol Biol* **421**, 160–171 (2012). URL http://dx.doi.org/10.1016/j.jmb.2012.02.031.

[39] Chiti, F., Stefani, M., Taddei, N., Ramponi, G. & Dobson, C. M. Rationalization of the effects of mutations on peptide and protein aggregation rates. *Nature* **424**, 805–808 (2003). URL http://dx.doi.org/10.1038/nature01891.

[40] Pawar, A. P. *et al.* Prediction of "aggregation-prone" and "aggregation-susceptible" regions in proteins associated with neurodegenerative diseases. *J Mol Biol* **350**, 379–392 (2005). URL http://dx.doi.org/10.1016/j.jmb.2005.04.016.

[41] Kim, W. & Hecht, M. H. Generic hydrophobic residues are sufficient to promote aggregation of the Alzheimer's Aβ42 peptide. *Proc Natl Acad Sci U S A* **103**, 15824–15829 (2006). URL http://dx.doi.org/10.1073/pnas.0605629103.

[42] Lührs, T. *et al.* 3D structure of Alzheimer's amyloid-beta(1-42) fibrils. *Proc Natl Acad Sci U S A* **102**, 17342–17347 (2005). URL http://dx.doi.org/10.1073/pnas.0506723102.

[43] Antzutkin, O. N. *et al.* Multiple quantum solid-state NMR indicates a parallel, not antiparallel, organization of beta-sheets in Alzheimer's beta-amyloid fibrils. *Proc Natl Acad Sci U S A* **97**, 13045–13050 (2000). URL http://dx.doi.org/10.1073/pnas.230315097.

[44] Petkova, A. T. *et al.* A structural model for Alzheimer's beta-amyloid fibrils based on experimental constraints from solid state NMR. *Proc Natl Acad Sci U S A* **99**, 16742–16747 (2002). URL http://dx.doi.org/10.1073/pnas.262663499.

[45] Danielsson, J., Jarvet, J., Damberg, P. & Gräslund, A. The Alzheimer beta-peptide shows temperature-dependent transitions between left-handed 3-helix, beta-strand and random coil secondary structures. *FEBS J* **272**, 3938–3949 (2005). URL http://dx.doi.org/10.1111/j.1742-4658.2005.04812.x.

[46] Chimon, S. *et al.* Evidence of fibril-like β-sheet structures in a neurotoxic amyloid intermediate of Alzheimer's β-amyloid. *Nat Struct Mol Biol* **14**, 1157–1164 (2007). URL http://dx.doi.org/10.1038/nsmb1345.

[47] Ahmed, M. *et al.* Structural conversion of neurotoxic amyloid-beta(1-42) oligomers to fibrils. *Nat Struct Mol Biol* **17**, 561–567 (2010). URL http://dx.doi.org/10.1038/nsmb.1799.

[48] Sandberg, A. *et al.* Stabilization of neurotoxic alzheimer amyloid-β oligomers by protein engineering. *Proc Natl Acad Sci U S A* **107**, 15595–15600 (2010). URL http://dx.doi.org/10.1073/pnas.1001740107.

[49] Necula, M., Kayed, R., Milton, S. & Glabe, C. G. Small molecule inhibitors of aggregation indicate that amyloid beta oligomerization and fibrillization pathways are independent and distinct. *J Biol Chem* **282**, 10311–10324 (2007). URL http://dx.doi.org/10.1074/jbc.M608207200.

[50] Wu, J. W. *et al.* Fibrillar oligomers nucleate the oligomerization of monomeric amyloid beta but do not seed fibril formation. *J Biol Chem* **285**, 6071–6079 (2010). URL http://dx.doi.org/10.1074/jbc.M109.069542.

[51] Fändrich, M. Oligomeric intermediates in amyloid formation: structure determination and mechanisms of toxicity. *J Mol Biol* **421**, 427–440 (2012). URL http://dx.doi.org/10.1016/j.jmb.2012.01.006.

[52] Lazo, N. D., Grant, M. A., Condron, M. C., Rigby, A. C. & Teplow, D. B. On the nucleation of amyloid beta-protein monomer folding. *Protein Sci* **14**, 1581–1596 (2005). URL http://dx.doi.org/10.1110/ps.041292205.

[53] Kayed, R. *et al.* Common structure of soluble amyloid oligomers implies common mechanism of pathogenesis. *Science* **300**, 486–489 (2003). URL http://dx.doi.org/10.1126/science.1079469.

[54] Hellstrand, E., Boland, B., Walsh, D. M. & Linse, S. Amyloid β-protein aggregation produces highly reproducible kinetic data and occurs by a two-phase process. *ACS Chem Neurosci* **1**, 13–18 (2010). URL http://dx.doi.org/10.1021/cn900015v.

[55] Ferrone, F. Analysis of protein aggregation kinetics. *Methods Enzymol* **309**, 256–274 (1999).

[56] Cohen, S. I. A. *et al.* Nucleated polymerization with secondary pathways. i. Time evolution of the principal moments. *J Chem Phys* **135**, 065105 (2011). URL http://dx.doi.org/10.1063/1.3608916.

[57] Cohen, S. I. A., Vendruscolo, M., Dobson, C. M. & Knowles, T. P. J. Nucleated polymerization with secondary pathways. ii. Determination of self-consistent solutions to growth processes described by non-linear master equations. *J Chem Phys* **135**, 065106 (2011). URL http://dx.doi.org/10.1063/1.3608917.

[58] Cukalevski, R. *et al.* Role of aromatic side chains in amyloid β-protein aggregation. *ACS Chem Neurosci* **3**, 1008–1016 (2012). URL http://dx.doi.org/10.1021/cn300073s.

[59] Bolognesi, B. *et al.* Ans binding reveals common features of cytotoxic amyloid species. *ACS Chem Biol* **5**, 735–740 (2010). URL http://dx.doi.org/10.1021/cb1001203.

[60] Garai, K. & Frieden, C. Quantitative analysis of the time course of aβ oligomerization and subsequent growth steps using tetramethylrhodamine-labeled aβ. *Proc Natl Acad Sci U S A* **110**, 3321–3326 (2013). URL http://dx.doi.org/10.1073/pnas.1222478110.

[61] Lomakin, A., Chung, D. S., Benedek, G. B., Kirschner, D. A. & Teplow, D. B. On the nucleation and growth of amyloid beta-protein fibrils: detection of nuclei and quantitation of rate constants. *Proc Natl Acad Sci U S A* **93**, 1125–1129 (1996). URL http://www.pnas.org/content/93/3/1125.abstract.

[62] Dobson, C. M. Protein chemistry. in the footsteps of alchemists. *Science* **304**, 1259–1262 (2004). URL http://dx.doi.org/10.1126/science.1093078.

[63] Härd, T. & Lendel, C. Inhibition of amyloid formation. *J Mol Biol* **421**, 441–465 (2012). URL http://dx.doi.org/10.1016/j.jmb.2011.12.062.

[64] Grönwall, C. *et al.* Selection and characterization of affibody ligands binding to alzheimer amyloid beta peptides. *J Biotechnol* **128**, 162–183 (2007). URL http://dx.doi.org/10.1016/j.jbiotec.2006.09.013.

[65] Hoyer, W., Grönwall, C., Jonsson, A., Ståhl, S. & Härd, T. Stabilization of a beta-hairpin in monomeric alzheimer's amyloid-beta peptide inhibits amyloid formation. *Proc Natl Acad Sci U S A* **105**, 5099–5104 (2008). URL http://dx.doi.org/10.1073/pnas.0711731105.

[66] Ehrnhoefer, D. E. *et al.* Egcg redirects amyloidogenic polypeptides into unstructured, off-pathway oligomers. *Nat Struct Mol Biol* **15**, 558–566 (2008). URL http://dx.doi.org/10.1038/nsmb.1437.

[67] Bieschke, J. *et al.* Small-molecule conversion of toxic oligomers to nontoxic β-sheet-rich amyloid fibrils. *Nat Chem Biol* **8**, 93–101 (2012). URL http://dx.doi.org/10.1038/nchembio.719.

[68] Lendel, C., Bolognesi, B., Wahlström, A., Dobson, C. M. & Gräslund, A. Detergent-like interaction of congo red with the amyloid beta peptide. *Biochemistry* **49**, 1358–1360 (2010). URL http://dx.doi.org/10.1021/bi902005t.

[69] Frid, P., Anisimov, S. V. & Popovic, N. Congo red and protein aggregation in neurodegenerative diseases. *Brain Res Rev* **53**, 135–160 (2007). URL http://dx.doi.org/10.1016/j.brainresrev.2006.08.001.

[70] Lorenzo, A. & Yankner, B. A. Beta-amyloid neurotoxicity requires fibril formation and is inhibited by congo red. *Proc Natl Acad Sci U S A* **91**, 12243–12247 (1994).

[71] Crowther, D. C. *et al.* Intraneuronal abeta, non-amyloid aggregates and neurodegeneration in a drosophila model of alzheimer's disease. *Neuroscience* **132**, 123–135 (2005). URL http://dx.doi.org/10.1016/j.neuroscience.2004.12.025.

[72] Masuda, M. *et al.* Small molecule inhibitors of alpha-synuclein filament assembly. *Biochemistry* **45**, 6085–6094 (2006). URL http://dx.doi.org/10.1021/bi0600749.

[73] Lendel, C. *et al.* On the mechanism of nonspecific inhibitors of protein aggregation: dissecting the interactions of alpha-synuclein with congo red and lacmoid. *Biochemistry* **48**, 8322–8334 (2009). URL http://dx.doi.org/10.1021/bi901285x.

[74] Feng, B. Y. *et al.* Small-molecule aggregates inhibit amyloid polymerization. *Nat Chem Biol* **4**, 197–199 (2008). URL http://dx.doi.org/10.1038/nchembio.65.

[75] Chen, J., Armstrong, A. H., Koehler, A. N. & Hecht, M. H. Small molecule microarrays enable the discovery of compounds that bind the alzheimer's aβ peptide and reduce its cytotoxicity. *J Am Chem Soc* **132**, 17015–17022 (2010). URL http://dx.doi.org/10.1021/ja107552s.

[76] Sievers, S. A. *et al.* Structure-based design of non-natural amino-acid inhibitors of amyloid fibril formation. *Nature* **475**, 96–100 (2011). URL http://dx.doi.org/10.1038/nature10154.

[77] Wahlström, A., Hugonin, L., Peralvarez-Marin, A., Jarvet, J. & Gräslund, A. Secondary structure conversions of Alzheimer's Aβ(1-40) peptide induced by membrane-mimicking detergents. *FEBS J* **275**, 5117–5128 (2008). URL http://dx.doi.org/10.1111/j.1742-4658.2008.06643.x.

[78] Kalyanasundaram, K. & Thomas, J. Environmental effects on vibronic band intensities in pyrene monomer fluorescence and their application in studies of micellar systems. *J Am Chem Soc* **99**, 2039–2044 (1977). URL http://pubs.acs.org/doi/abs/10.1021/ja00449a004.

[79] Goddard, E. D., Turro, N. J., Kuo, P. L. & Ananthapadmanabhan, K. P. Fluorescence probes for critical micelle concentration determination. *Langmuir* **1**, 352–355 (1985). URL http://dx.doi.org/10.1021/la00063a015.

[80] Jarvet, J., Danielsson, J., Damberg, P., Oleszczuk, M. & Gräslund, A. Positioning of the Alzheimer Aβ(1-40) peptide in SDS micelles using NMR and paramagnetic probes. *J Biomol NMR* **39**, 63–72 (2007). URL http://dx.doi.org/10.1007/s10858-007-9176-4.

Appendices

A Redfield equation

The Hamiltonian may be divided into a time-independent and -dependent part $\hat{H}_0$ and $\hat{H}_1(t)$, respectively. Thus, defining the *Liouvillian* operator $\hat{L}(t) = [\hat{H}(t), \ ]$ the LvN equation is expressed as [13, 22]:

$$\frac{d\rho(t)}{dt} = -i\left[\hat{H}_0 + \hat{H}_1(t), \rho(t)\right] = -i\left(\hat{L}_0 + \hat{L}_1(t)\right)\rho(t) \tag{17}$$

The equation is transformed into the interaction frame by:

$$\rho^T(t) = \exp(i\hat{L}_0 t)\rho(t) = \exp(i\hat{H}_0 t)\rho(t)\exp(-i\hat{H}_0 t) \tag{18}$$

Hence, the LvN equation yields:

$$\frac{d\rho^T(t)}{dt} = i\hat{L}_0\exp(i\hat{L}_0 t)\rho(t) + \exp(i\hat{L}_0 t)\frac{d\rho(t)}{dt} \tag{19a}$$

$$= i\exp(i\hat{L}_0 t)\hat{L}_0\rho(t) + \exp(i\hat{L}_0 t)\left(-i\left(\hat{L}_0 + \hat{L}_1(t)\right)\rho(t)\right) \tag{19b}$$

$$= -i\exp(i\hat{L}_0 t)\hat{L}_1(t)\rho(t) = -i\left(\hat{L}_1(t)\rho(t)\right)^T \tag{19c}$$

$$= -i\left[\hat{H}_1^T(t), \rho^T(t)\right] \tag{19d}$$

This differential equation may be solved by integration over a time period t:

$$\rho^T(t) = \rho^T(0) - i\int_0^t \left[\hat{H}_1^T(t'), \rho^T(t')\right] dt' \tag{20}$$

As $\rho^T(t')$ is not known the solution may be approximated, using the variable substitution $\tau = t' - t$, which yields [13]:

$$\rho^T(t) = i\left[\rho^T(0), \hat{H}_1^T(t')\right] - \int_0^t \left[\hat{H}_1^T(t), \left[\hat{H}_1^T(t+\tau), \rho^T(0)\right]\right] d\tau \tag{21}$$

The system may be described as an ensemble of ensembles which implies that the average of $\hat{H}_1(t)$ over the ensemble of ensembles is zero at every given time point. Thus, the first commutator in eq(21) vanishes. Using several additional approximations [13, 22], equation (21) becomes the *Redfield* equation formulated in eq(8).